Published in final edited form as:

Nature. 2013 December 19; 504(7480): 456–459. doi:10.1038/nature12723.

The Heterotaxy gene, GALNT11, glycosylates Notch to orchestrate cilia type and laterality

Marko T. Boskovski[1,2,*], **Shiaulou Yuan**[1,*], **Nis Borbye Pedersen**[3], **Christoffer Knak Goth**[3], **Svetlana Makova**[1], **Henrik Clausen**[3], **Martina Brueckner**[1], and **Mustafa K. Khokha**[1,4]

[1]Program in Vertebrate Developmental Biology, Department of Pediatrics and Genetics, Yale University School of Medicine, 333 Cedar Street, New Haven CT 06520

[3]Copenhagen Center for Glycomics, Department of Cellular and Molecular Medicine, Faculty of Health Sciences, University of Copenhagen, Building 24.6.30, Blegdamsvej 3, DK-2200 Copenhagen N, Denmark

Abstract

Heterotaxy (Htx) is a disorder of left-right (LR) body patterning, or laterality, that is associated with major congenital heart disease[1]. The etiology and mechanism underlying most human Htx is poorly understood. In vertebrates, laterality is initiated at the embryonic left-right organizer (LRO), where motile cilia generate leftward flow that is detected by immotile sensory cilia, which transduce flow into downstream asymmetric signals[2–6]. The mechanism that specifies these two cilia types remains unknown. We now show that the GalNAc-type O-glycosylation enzyme GALNT11 is crucial to such determination. We previously identified GALNT11 as a candidate disease gene in a patient with Htx[7], and now demonstrate, in *Xenopus*, that *galnt11* activates Notch signaling. GALNT11 O-glycosylates NOTCH1 peptides *in vitro*, thereby supporting a mechanism of Notch activation either by increasing ADAM17-mediated ectodomain shedding of the Notch receptor or by modification of specific EGF repeats. We further developed a quantitative live imaging technique for *Xenopus* LRO cilia and show that *galnt11*-mediated *notch1* signaling modulates the spatial distribution and ratio of motile and immotile cilia at the LRO. *galnt11* or *notch1* depletion increases the ratio of motile cilia at the expense of immotile cilia and produces a laterality defect reminiscent of loss of the ciliary sensor Pkd2. In contrast, Notch overexpression decreases this ratio mimicking the ciliopathy, primary ciliary dyskinesia. Together, our data demonstrate that Galnt11 modifies Notch, establishing an essential balance between motile and immotile cilia at the LRO to determine laterality and identifies a novel mechanism for human Htx.

[4]Correspondence and requests for materials should be addressed to mustafa.khokha@yale.edu.

[2]Present Address: Department of Surgery, Brigham and Women's Hospital, Harvard Medical School, 75 Francis St, Boston MA 02115

[*]these authors contributed equally to this work

Author Contributions

MTB, SY, SM, MB, and MKK conceived and designed the embryological experiments in *Xenopus* and mouse. MTB, SY, SM, and MKK performed the *Xenopus* experiments while MB performed mouse experiments. NBP, CKG and HC performed and evaluated the glycosylation and ADAM studies. All authors wrote and contributed to the manuscript.

The authors declare no competing financial interests.

Keywords

live imaging; *Xenopus tropicalis*; left-right patterning; O-glycosylation; congenital heart disease; motility; mechanosensation; primary cilium; mouse node; gastrocoel roof plate; GalNAcT11

Recent, genomic analyses have identified candidate genes for congenital heart disease[7–9]; however, determining disease causality and developmental mechanisms remains challenging. In a Htx patient, we identified a copy number deletion of the *GALNT11* gene[7], a polypeptide N-acetylgalactosaminyltransferase (GALNT) that controls the initiation of GalNAc-type O-glycosylation[10]. GALNTs serve different functions; however, a role for GALNT11 in vertebrate development is unknown.

To investigate the role of GALNT11 in LR development, we first examined its effects on cardiac looping. Normally, in vertebrates, the initially midline heart tube forms a rightward (D) loop. Aberrant LR patterning results in abnormal cardiac loops, including leftward (L) and symmetric/midline (A) loops. In *Xenopus*, we first confirmed that *galnt11* knockdown (KD) by morpholino oligonucleotide (MO) led to abnormal cardiac looping, and that overexpression of human *GALNT11* mRNA could rescue this phenotype, demonstrating specificity (Fig 1a).

We then examined early markers of LR patterning, *dand5 (coco, cerl2)* and *pitx2c*. *coco* is the earliest known asymmetric marker[11]. At the LRO, *coco* expression is initially symmetric but develops a right-sided bias with the onset of cilia-driven flow, while *pitx2c* is expressed in the left lateral plate mesoderm[11]. Both *galnt11* KD and GALNT11 GOF resulted in abnormal patterns of *coco* and *pitx2c*, indicating that *galnt11* affects LR patterning upstream of *coco* at the ciliated LRO (Fig 1b). Consistent with this finding, we previously found *galnt11* mRNA expressed at the LRO[7], and Galnt11 protein is localized in the mouse LRO (node), with enrichment in crown cells compared to pit cells (Ext Fig 1).

Abnormal *coco* expression suggests an abnormality in cilia-dependent signaling at the LRO. We first searched for a ciliary ultrastructural defect in the multiciliated cells on the *Xenopus* epidermis but found no consistent defect (Ext Fig 2). However, we did observe a higher density of multiciliated cells (compare Fig 1c and 1d). Conversely, *galnt11* GOF reduced the number of multiciliated cells (Fig 1e, 1f). Interestingly, a similar phenotype is seen with disruptions in Notch signaling[12]. Like *galnt11*, *notch1* KD increases, while *notch1* GOF (*nicd*) decreases, the multiciliated cell density (Fig 1g–j). Based on these results, we hypothesized that *galnt11* may affect the Notch signaling pathway.

We further explored this possibility by examining the effects of *galnt11* and *notch1* on the LR developmental cascade. *galnt11* and *notch1* KD and GOF produced similar LR patterning defects (Ext Fig 3), suggesting that *galnt11* affects Notch signaling directly or in a parallel pathway. Notch is a key regulator of many aspects of biology[13]. The core components of the Notch pathway include a ligand, *Delta* or *Jagged*, the transmembrane Notch receptor, and the CBF1/Su(H)/Lag-1 (CSL) transcription factor complex (Fig 1k). Signaling from the Notch receptor requires a number of cleavage steps, S1–S3, culminating

in the release of the Notch intracellular domain (NICD), which translocates to the nucleus, interacts with CSL, and modulates Notch responsive genes (Fig 1k).

To test if Galnt11 acts directly in the Notch pathway, we attempted to rescue the *galnt11* KD phenotype with Notch pathway members. Using *pitx2c* as our assay, we found that *delta* GOF had little effect on *galnt11* KD, but both *nicd* and *su(h)-ank* (a constitutively active CSL protein[14]) efficiently rescued the phenotype (Fig 1l).

Notch functions are regulated by different O-glycosylations in the EGF repeats of the Notch receptor that affect the ligand-receptor interaction[15]. However, GalNAc-type O-glycosylation has not been reported previously; given our results, we searched for GalNAc-type O-glycosylation of Notch to identify activation mechanisms. First, we confirmed that *Xenopus* and human GALNT11 have identical substrate specificity similar to the *Drosophila* ortholog (Ext Table 1)[16]. Using mass spectrometry, we then tested 38 peptides derived from the extracellular domain (ECD) of human NOTCH1 in an *in vitro* enzyme assay to identify potential substrate sites for GALNT11 O-glycosylation. Three peptides were glycosylated by GALNT11, two in EGF repeats 6 and 36 overlapping proposed O-fucosylation sites[15] and one in the juxtamembrane region near the ADAM metalloproteinase ectodomain shedding site (Fig 2a)[17]. The identified peptide substrates and several others were also glycosylated by other GALNTs (Ext Fig 4).

Our experiments in *Xenopus* indicate that *galnt11* activates the Notch pathway (Fig 1 and Ext Fig 3). However, the identified O-glycosylation site adjacent to the ADAM processing site (Fig 2a) would be expected to *inhibit* cleavage (based on numerous previous examples e.g. in TNR16, Ext Fig 5a)[18] and thus *block* Notch receptor activation (Fig 1k). Surprisingly, but in support of our original hypothesis, GALNT11 O-glycosylation enhanced cleavage of the juxtamembrane peptide by ADAM 17 (Fig. 2b–d, Ext Fig 5b). We thus propose a model where site-specific GALNT11 glycosylation of NOTCH1 adjacent to the ADAM cleavage site facilitates shedding and activates the pathway by increasing the amount of NICD. However, alternative models remain possible with the identified glycosylation of ECD peptides, and additional *in vivo* studies are needed. Notably, the catalytic function of GALNT11 is required for mediating LR development, since mutation of essential catalytic residues from DSH to DSA (H247A)[10] eliminates the aberrant effects on *pitx2c* and LR looping seen with wildtype GALNT11 GOF (Ext Fig 5c,d).

Next, we focused on how Galnt11 modulation of Notch1 alters LR development, where Notch has several possible roles[19]. Our data indicate that *galnt11* acts upstream of asymmetric *coco* expression, so we focused our attention on the potential relationship between *galnt11* and cilia function in the LRO.

galnt11 morphants retained bilateral symmetry: a predominance of midline, cardiac A loops and symmetric *coco* and *pitx2* expression (Fig1 and Ext Fig 3). Similarly, our patient with *GALNT11* haploinsufficiency had bilateral symmetry, presenting with right atrial isomerism[7]. Finally, mutant *Dll1* or *Notch1/2* mice and *des/notch1a* zebrafish are also predominately symmetric[20,21]. This is reminiscent of the *Pkd2* mutant mice phenotype, which has right isomerism due to failure of ciliary sensing[4,22]. In contrast, overexpression of

GALNT11 in *Xenopus* led to L and D loops (Fig 1a), and randomization across the LR axis, mimicking the human disorder primary ciliary dyskinesia, where ineffective ciliary beating fails to generate extracellular fluid flow. Based on these two observations, we postulated that GALNT11 via Notch specifies immotile (sensory) versus motile cilia (Ext Fig 8).

To test this, we developed a live imaging method to simultaneously assay motile and immotile cilia in the LRO of *Xenopus*, the gastrocoel roof plate (GRP). Employing an epitope-tagged ciliary protein, Arl13b-mCherry[23] with confocal microscopy (Fig 3a, Sup Video 1), we spatially mapped motile and immotile cilia. After additive analysis of numerous LROs, we qualitatively and quantitatively analyzed cell populations with either cilia type (Ext Fig 6a–d). In wildtype *Xenopus* LRO explants, we found that motile cilia are concentrated in the center, with relatively more immotile cilia at the periphery, similar to the mouse LRO (or node) pit and crown, respectively (Fig 3b, c, h [vehicle])[3,4]. In both locations, cilia types are intermixed similar to the mouse LRO.

To evaluate the role of *notch1* signaling, we co-injected *nicd* and *arl13b-mCherry* and analyzed cilia types. *nicd* overexpression reduced the ratio of motile to immotile cilia when compared to controls (compare Fig 3d to b, 3g and Sup Video 2). KD of *notch1* or *galnt11* had the opposite effect, increasing the ratio of motile to immotile cilia (Fig 3e–g and Sup Video 3,4). Previous reports have identified asymmetric RNA expression of Notch ligands at the LRO[24]; however, we failed to observe any significant asymmetry in cilia number or type across the LR axis of the LRO (Ext Fig 6j,k).

The transcription factors, FoxJ1 and Rfx2 are regulators of motile ciliogenesis[25–27] so we evaluated the expression of *rfx2* and *foxj1* at the *Xenopus* LRO in response to Notch activation. *nicd* or *GALNT11* GOF reduced the expression of *foxj1* and *rfx2*, while H247A GALNT11 GOF had no effect (Ext Fig 7a–h), suggesting that Notch signaling functions upstream of *foxj1* and *rfx2* in determining ciliary type at the LRO.

Since Galnt11 expression in the mouse node was most prominent in the lateral crown cells (Ext Fig 1), we compared the *Xenopus* LRO periphery with the center (Ext Fig 6a–h). Interestingly, cilia in the periphery, where they are predominantly immotile (Fig 3b, c), were strikingly transformed to the motile type with *galnt11* and *notch1* KD (Fig 3h). Overall, mean total cilia numbers per LRO were not statistically different, supporting altered cilia identity as the primary mechanism for LR defects (Ext Fig 6i). To confirm that *galnt11* was not perturbing formation of the LRO periphery, we tested peripheral markers at stages prior to when flow alters *coco* and noted no significant differences (Ext Fig 7i–u). We conclude that Galnt11/Notch1 signaling mediates a critical switch between these two cilia types and their spatial distribution within the LRO (Ext Fig 8).

Our results strengthen the two cilia model of LR patterning by identifying a signaling pathway that modulates the balance between motile and immotile cilia[3] at the LRO (Ext Fig 8). Exactly how many cilia and which types are needed for proper LR signaling is controversial and may depend on the specific architecture of the LRO found in each organism. For example, in the mouse LRO, a partially open cup-shaped structure, only two motile cilia are needed for LR patterning[28]. However, in the zebrafish LRO, which is an

enclosed spherical structure, there appears to be a greater enrichment of motile cilia relative to frog or mouse[29]. In the frog LRO, which is a shallow indentation inside the gastrocoel cavity, motile cilia are required only on the left for correct LR patterning[30]. For immotile cilia, there may be a threshold number that also differs depending on the specific architecture of the organism's LRO. Further studies will need to address why two cilia types are needed in the LRO and the mechanisms that convert ciliary sensation of flow to asymmetric gene expression and laterality.

Our findings were prompted by gene discovery in a single disease subject. We had no additional alleles to prove causality using a genetic approach[7]. Instead, we assayed for phenocopy in a high-throughput vertebrate model, *Xenopus*, and then embarked on mechanistic analyses in order to understand the role GALNT11 plays in LR patterning and disease. Our results have led to new insights into the basic biology of GalNAc-type O-glycosylation, Notch signaling, LR patterning, and the etiology of Htx. Because of high locus heterogeneity and severe reduction in fitness, causative gene discovery in children with birth defects has been challenging. However, with the brisk pace of advancing human genomics, these limitations are being broken, and new opportunities are at hand to understand birth defects and their underlying genetic mechanisms especially when coupled with rapid vertebrate developmental models such as *Xenopus*.

Methods

Frog Husbandry

X. tropicalis were housed and cared for in our aquatics facility according to established protocols that were approved by Yale IACUC.

Mouse Husbandry

Mice were housed and cared for in our animal facility according to established protocols that were approved by Yale IACUC.

Microinjection of MOs and mRNA in *Xenopus*

We induced ovulation and collected eggs according to established protocols[31]. Staging of *Xenopus* tadpoles were according to Nieuwkoop and Faber[32]. MOs or mRNA were injected into the one cell or two cell embryo as previously described[33]. The following morpholino oligos were injected: *galnt11* splice blocking (0.5–1 ng 5'CAGGTCAGAGAGAAGGGCACCTACT), *galnt11* ATG blocking (0.5–1 ng 5'GCGCTGCCCATCGTCCCCCTAGCA), *notch1* (3 ng 5'GAACAAGCAGCCCGATCCGATACAT), *dnah9* (2–4 ng 5'TGGGTCACTCATCTTTCCCCTCATT). Alexa488 (Invitrogen), mini-ruby (Invitrogen), or GFP (100pg) were injected as tracers. We generated *in vitro* capped mRNA using mMessage machine kit (Ambion) and followed the manufacturer's instructions. We generated human *GALNT11* mRNA by cloning the insert from IMAGE clone 100068224 into the pCSDest vector using Gateway recombination techniques. To generate *arl13b-mCherry* mRNA, we fused zebrafish *arl13b* to *mCherry* into the pCSDest2 vector using Gateway recombination techniques. We injected 6 pg of *GALNT11* mRNA for rescue of

galnt11 morphants, 25 pg of *GALNT11* mRNA for overexpression to assay LR patterning and in the ciliated epidermis assay, 25 pg *GALNT11 H247A*, 12.5 pg of *nicd* mRNA for rescue of *galnt11* morphants, 25 pg of *nicd* mRNA for overexpression to assay LR patterning and in the ciliated epidermis assay, 2 pg of *su(h)ank*, and 100–200 pg of *arl13b-mCherry*.

Cardiac looping in *Xenopus*

Frog embryos at stage 45 were treated with benzocaine and ventrally scored for cardiac looping using a light dissection microscope. Loop direction is defined by the position of the outflow tract relative to the inflow of the heart: outflow to the right – D loop; outflow to the left – L loop; outflow midline – A loop.

Transfection of IMCD3 cells

Cells were transfected with Lipofectamine 2000 (Invitrogen) according to manufacturer's instructions. Cells were fixed in 4% PFA 48 hours after transfection and processed for immunofluorescence. Cells were not authenticated nor tested for mycoplasma contamination.

Immunofluorescence (IF) and *in situ* hybridization

E8.0 mouse embryos were harvested from timed pregnancies for node IF. Observation of coital plug marks e0.5. For GRPs, we collected stage (st) 14 *Xenopus* embryos for *foxj1* and *rfx2*, st 16 for *coco, xnr1, and gdf3*, and st. 19–21 for *coco*. For *pitx2c*, we collected *Xenopus* embryos at st 28–31. For IF of multiciliated epidermal cells, we used st. 28–30 *Xenopus* embryos. GRPs were dissected as previously described[5].

For IF, transfected mammalian cells, mouse and *Xenopus* embryos were fixed in 4% paraformaldehyde/PBS overnight at 4°Mouse embryos, *Xenopus* embryos, and *Xenopus* GRPs were labeled by immunofluorescence as previously described[3,33]. All embryos were mounted in Pro-Long Gold (Invitrogen) prior to imaging. Imaging was performed on a Zeiss Axiovert microscope equipped with Apotome optical interference imaging to obtain optical sections. For comparison of left- and right-sided epithelial cilia density, the *Xenopus* embryos were sandwiched between two coverslips and each side of a single embryo was imaged.

RNA *in-situ* hybridization was done as previously described[33]. We detected *coco*[34], *gdf3, foxj1, pitx2c, rfx2, and xnr1* by generating anti-digoxigenin probes (Roche) using clones TEgg007d24, Tgas141F11, TNeu058M03, TNeu083k20, IMAGE:7680423, and TGas124h10 respectively.

Antibodies used

Anti-Arl13b[35]

Rabbit anti-Arl13b (1:500, courtesy of T. Caspary)

Anti-acetylated tubulin (Sigma, Catalog: T-6793)[36]

Mouse monoclonal anti-acetylated tubulin, clone 6-11B-1 (1:1000)

Species reactivity: monkey, Protista, mouse, pig, human, bovine, invertebrates, rat, hamster, plant, frog, chicken

Anti-GALNT11 (Santa Cruz, Catalog: sc-68498)

Goat polyclonal anti-GALNT11 (K-19) (1:200) (transfected cells)

Species reactivity: mouse, rat, human

Anti-GALNT11[37]

Mouse, polyclonal (undiluted) (mouse LRO)

Live imaging of cilia motility in the GRP

For imaging of cilia motility in the GRP, wildtype embryos were injected with *arl13b-mCherry* mRNA at the 1-cell stage and then cultured until stage 16 – 17. Vehicle embryos were co-injected with water, while *nicd* overexpressants, *notch1* morphants, and *galnt11* morphants were co-injected with RNA or MOs. GRP explants were prepared in MBSH and mounted on a coverglass within a ring of petroleum jelly. High-speed fluorescent imaging was performed on an LSM 710 DUO (Zeiss) microscope equipped with a rapid LIVE linescan detector, a 40× C-Apochromat water objective and a 561-nm laserline. Multiple rapid acquisitions were collected per each embryo at several Z-planes within the GRP. All acquisitions were collected at a rate of 240 frames per second (fps) with a 512 × 512 pixel resolution using maximal pinhole settings, bidirectional scanning and 0 binning in Zen 2010 (Zeiss). Cilia beating dynamics were analyzed and quantified by kymographs in ImageJ (NIH) with an elapsed time of 1s displayed in Fig 3. Movie clips with overlays were prepared using Final Cut (Apple) and Compressor (Apple).

Spatial analysis of motile and immotile cilia populations in the GRP

Live high-speed acquisitions of GRP explants expressing *arl13b-mCherry* were slowed down, played back, and scored for motile and immotile cilia in ImageJ (NIH) onto two overlaying images: one for motile and the second for immotile cilia (Ext Fig 6a–c). Each overlaying image was converted into a binary image and then converted a second time into a false-colored 8-bit image. Both images were then merged to generate a two-color map of cilia distribution for an individual GRP (Ext Fig 6d). For each experimental condition, numerous two-color maps were assembled into an image series and processed into a single composite image using the projection function in ImageJ (Fig 3b, d, e, f). For quantification of motile and immotile cilia in the periphery or center region of the LRO, a two-color map representing a single GRP was imported into Photoshop CS5 (Adobe). A new layer (named ‘Layer 1’) was created and the edge of the total ciliated population of that GRP was traced using the pencil tool (Ext Fig 6e). A duplicate of the trace layer was created (named ‘Layer 2’), decreased in area uniformly (to maintain the shape of the original trace) by 50% using the transform tool and aligned at the absolute center of Layer 1 (Ext Fig 6f). By dividing the LRO into two 50% areas, while maintaining the specific shape of each GRP, the periphery and center of the LRO were defined with equal areas; thus minimizing any potential pre-conceived size bias for either zone (Ext Fig 6g, h). Further, this estimate is broadly supported by studies of the crown and pit cells in the mouse LRO[4]. The area within the trace

in Layer 2 was defined as the center of the LRO, while the area between the traces in Layers 1 and 2 was defined as the periphery. Motile, immotile cilia, and total cilia (Fig 3, Ext Fig 6i) were scored specifically in the center and then periphery area.

In vitro GALNT11 glycosylation and ADAM processing studies

Glycosylation assays were performed in 25 μL reaction mixtures containing 10 μg peptide substrate, 4 mM UDP-GalNAc, 25 mM cacodylic acid sodium (pH 7.4), 10 mM $MnCl_2$, 0.25% Triton X-100, and purified recombinant GALNT enzymes (0.1 μg). The enzyme reactions in Fig 2a were performed with GALNT11 by *in vitro* assays for 18–24 hrs. ADAM cleavage assays were performed with 250 nM ADAM17 (Enzo Life Sciences) with 10 μg of peptide or GalNAc-glycopeptide substrate in 25 mM TRIS (pH 9) in a total volume of 25 μl. Reaction for ADAM cleavage assays were sampled at 0 hrs, 15 min, 1 hrs, and 2 hrs. All reactions were incubated at 37°C and product development evaluated by MALDI-TOF in a time-course as previously described[37] except that a Bruker Autoflex MALDI-TOF instrument with accompanying Compass 1.4 FlexSeries software was used for product evaluation. Position of sites were determined by electrospray ionization-linear ion trap-Fourier transform mass spectrometry (ESI-LIT-FT-MS) applying both high energy collision-induced dissociation and electron transfer dissociation (ETD) enabling peptide sequence analysis by MS/MS (MS^2) with retention of glycan site-specific fragments as described in detail previously[38] (data not shown). HPLC analyses were performed using a multistep gradient on a Dionex Ultimate 3000 LC system (Thermo Scientific) with a Kinetex 2.6u C18 100A 100×4.60 mm column (Phenomenex). Areas under the curves were calculated using the Chromeleon 6.80 software. Statistical analysis (two-tailed T-test) was carried out in Microsoft Excel comparing the averages of full-length glycosylated and unglycosylated peptides from three different sets of cleavage experiments. Statistical analysis showed that the difference in cleavage efficiency between the unglycosylated and glycosylated peptides was significant ($p<0.05$) in Fig 2c.

Electron microscopy

Stage 27 *Xenopus* embryos were fixed with Karnovsky fixative for 1 h at 4°C, washed with 0.1 M sodium cacodylate, pH 7.4, then post-fixed with Palade's osmium for 1 h at 4°C, shielded from light. Following a second wash, embryos were stained with Kellenburger's solution for 1 h at RT, washed in double distilled water, then put through an ethanol series, propylene oxide, 50/50 propylene oxide/epon, then two incubations in 100% epon. Embedded embryos were sectioned at 400 nm before staining with 2% uranyl acetate. Micrographs were taken on a Zeiss 910 electron microscope.

Statistical Analysis

We estimated that for *Xenopus* experiments 20–25 samples per experimental condition were necessary for statistical significance given the magnitude of the changes expected. In most cases, considerably more samples were obtained for each except as noted in the figures. Statistical significance is reported as appropriate. In no cases did we exclude samples except in cases of technical failure (embryos were found to be uninjected, *in situ* hybridization failed, etc). We did not use any randomization method. For *pitx2* and *coco* expression, one

observer was unblinded but in all cases at least 1–2 other observers were blinded and a high degree of concordance was noted.

For Fig 1a sample sizes were 130 for uninjected controls, 145 for *Galnt11* start MO, 105 for *Galnt11* splice MO, 83 for *Galnt11* splice MO + *Galnt11* RNA, and 96 for *Galnt11* RNA. These numbers represent the cumulative total of three biological replicates. For Fig 1b *coco* expression patterns sample sizes were 21 for uninjected controls, 21 for *Galnt11* splice MO, and 23 for *Galnt11* RNA. For *pitx2c* expression patterns sample sizes were 45 for uninjected controls, 54 for *Galnt11* splice MO, and 34 for *Galnt11* RNA. These numbers represent the cumulative total of two biological replicates for *coco* and three for *pitx2* expression patterns. For Fig 1l sample sizes were 96 for uninjected controls, 78 for *Galnt11* MO, 65 for *Galnt11* MO + delta, 86 for *Galnt11* MO + *nicd*, and 62 for *Galnt11* MO + *Su(h)ank*. These numbers represent the cumulative total of three biological replicates.

For Fig 2, enzyme reactions were repeated three times, and statistical analysis on HPLC data was done using three biological replicates.

For the entirety of Fig 3, the data shown represent a cumulative total of 15 biological replicates. Fig 3a is a representative image. For Fig 3b,d,e,f, the analyzed samples sizes were 8 embryos per each condition. For Fig 3g,h, analyzed sample sizes were 17 embryos for vehicle (dH_20), 12 for *nicd* RNA, 12 for *notch1* MO and 15 for *galnt11* MO. For Fig 3g,h, statistical significance was analyzed by t-test (two-tailed, type two); center values represent averages; errors bars indicate standard error. For quantitative analysis and mapping, embryos were excluded on the following pre-established criteria: 1) only partial labeling of total cilia population in the GRP by Arl13b-mCherry; 2) improper embryonic stage (stages 16/17 were defined as the inclusion criteria).

For Ext Fig 3 *coco* expression patterns sample sizes were 21 for uninjected control, 24 for *galnt11* MO, 30 for *notch* MO, 23 for *galnt11* RNA, and 22 for *nicd* RNA. These numbers represent the cumulative total of two biological replicates. For *pitx2c* expression patterns, sample sizes were 45 for uninjected control, 54 for *galnt11* MO, 50 for *notch* MO, 34 for *galnt11* RNA, and 30 for *nicd* RNA. These numbers represent the cumulative total of three biological replicates. For heart looping sample sizes were 276 for uninjected control, 68 for *galnt11* MO, 75 for *notch* MO, 91 for *galnt11* RNA, and 50 for *nicd* RNA.

For Ext Fig 4 glycosylations reactions were all repeated a minimum of two times for each glycosylation enzyme.

For Ext Fig 5, panel a) is a representative spectrum of three independent experiments, and b) is a representative spectrum of two independent experiments. For panel c) *pitx2c* expression patterns sample sizes were 45 for uninjected control, 34 for *galnt11* RNA and 40 for *galnt11* H247A RNA. These numbers represent the cumulative total of two biological replicates. For heart looping sample sizes were 276 for uninjected control, 91 for *galnt11* RNA and 133 for *galnt11* H247A RNA. These numbers represent the cumulative total of 3 biological replicates.

For the entirety of Ext Fig 6, the data shown represent a cumulative total of 15 biological replicates. Ext Fig 6a–h are representative images. For Ext Fig 6i, analyzed sample sizes were 17 embryos for vehicle (dH_20), 12 for nicd RNA, 12 for notch1 MO and 15 for galnt11 MO. For Ext Fig 6j,k, analyzed sample sizes were 17 vehicle ('wildtype') embryos. For Ext Fig 6i,j,k, statistical significance was analyzed by t-test (two-tailed, type two); center values represent averages; errors bars indicate standard error. For quantitative analysis and mapping, embryos were excluded on the following pre-established criteria: 1) only partial labeling of total cilia population in the GRP by Arl13b-mCherry; 2) improper embryonic stage (stages 16/17 were defined as the inclusion criteria).

In all figures, statistical significance was defined as $P<0.05$, while $P\geq0.05$ was defined as not significant (NS). A single asterisk indicates $P<0.05$, while double and triple asterisks indicates $P<0.01$ and $P<0.001$, respectively. Fig 3 and Ext Fig 6 were analyzed by t-test (two-tailed, type two) presuming a normal distribution. Fig 1, Ext Fig 3, Ext Fig 5 were analyzed by chi-square as previously described[39].

Supplementary Material

Refer to Web version on PubMed Central for supplementary material.

Acknowledgments

We thank the patients and their families who are the inspiration for this study. We thank S. Kubek and M. Slocum for animal husbandry. We thank U. Mandel, M. Vester-Christensen, T. D. Madsen, and S. B. Levery for help with generation of polyclonal antibodies, recombinant GALNT enzymes, *in vitro* glycosylation experiments, and mass spectrometry. Thanks to the Center for Cellular and Molecular Imaging at Yale for assistance with SEM/TEM (C. Rahner and M. Graham) and confocal imaging. Thanks to C. Kintner and Z. Sun for reagents. Thanks to R. Harland, K. Liem, R. Lifton, J. McGrath, A. Horwich and Z. Sun for critical reading of the manuscript. MTB was supported by Grant Number TL 1 RR024137 from NCRR/NIH and NIH Roadmap for Medical Research. SY was supported by NIH training grant 5T32HD00709436. This work was supported by NIH R01HL093280 to MB and NIH DE018825, DE018824 to MKK, and the Danish National Research Foundation (DNRF107) to HC.

References

1. Sutherland MJ, Ware SM. Disorders of left-right asymmetry: heterotaxy and situs inversus. Am J Med Genet C Semin Med Genet. 2009; 151C:307–317. [PubMed: 19876930]
2. Nonaka S, et al. Randomization of left-right asymmetry due to loss of nodal cilia generating leftward flow of extraembryonic fluid in mice lacking KIF3B motor protein. Cell. 1998; 95:829–837. [published erratum appears in Cell 1999 Oct 1;99(1):117]. [PubMed: 9865700]
3. McGrath J, Somlo S, Makova S, Tian X, Brueckner M. Two populations of node monocilia initiate left-right asymmetry in the mouse. Cell. 2003; 114:61–73. [PubMed: 12859898]
4. Yoshiba S, et al. Cilia at the node of mouse embryos sense fluid flow for left-right determination via Pkd2. Science. 2012; 338:226–231. [PubMed: 22983710]
5. Schweickert A, et al. Cilia-driven leftward flow determines laterality in Xenopus. Curr Biol. 2007; 17:60–66. [PubMed: 17208188]
6. Kramer-Zucker AG, et al. Cilia-driven fluid flow in the zebrafish pronephros, brain and Kupffer's vesicle is required for normal organogenesis. Development. 2005; 132:1907–1921. [PubMed: 15790966]
7. Fakhro KA, et al. Rare copy number variations in congenital heart disease patients identify unique genes in left-right patterning. Proc Natl Acad Sci USA. 2011; 108:2915–2920. [PubMed: 21282601]

8. Greenway SC, et al. De novo copy number variants identify new genes and loci in isolated sporadic tetralogy of Fallot. Nat Genet. 2009; 41:931–935. [PubMed: 19597493]
9. Zaidi S, et al. De novo mutations in histone-modifying genes in congenital heart disease. Nature. 2013; 498:220–223. [PubMed: 23665959]
10. Bennett EP, et al. Control of mucin-type O-glycosylation: a classification of the polypeptide GalNAc-transferase gene family. Glycobiology. 2012; 22:736–756. [PubMed: 22183981]
11. Schweickert A, et al. The nodal inhibitor Coco is a critical target of leftward flow in Xenopus. Curr Biol. 2010; 20:738–743. [PubMed: 20381352]
12. Deblandre GA, Wettstein DA, Koyano-Nakagawa N, Kintner C. A two-step mechanism generates the spacing pattern of the ciliated cells in the skin of Xenopus embryos. Development. 1999; 126:4715–4728. [PubMed: 10518489]
13. Artavanis-Tsakonas S, Muskavitch MA. Notch: the past, the present, and the future. Curr Top Dev Biol. 2010; 92:1–29. [PubMed: 20816391]
14. Wettstein DA, Turner DL, Kintner C. The Xenopus homolog of Drosophila Suppressor of Hairless mediates Notch signaling during primary neurogenesis. Development. 1997; 124:693–702. [PubMed: 9043084]
15. Rana NA, Haltiwanger RS. Fringe benefits: functional and structural impacts of O-glycosylation on the extracellular domain of Notch receptors. Curr Opin Struct Biol. 2011; 21:583–589. [PubMed: 21924891]
16. Schwientek T, et al. Functional conservation of subfamilies of putative UDP-N-acetylgalactosamine:polypeptide N-acetylgalactosaminyltransferases in Drosophila, Caenorhabditis elegans, and mammals. One subfamily composed of l(2)35Aa is essential in Drosophila. J Biol Chem. 2002; 277:22623–22638. [PubMed: 11925450]
17. Brou C, et al. A novel proteolytic cleavage involved in Notch signaling: the role of the disintegrin-metalloprotease TACE. Mol Cell. 2000; 5:207–216. [PubMed: 10882063]
18. Gram Schjoldager KT, et al. A systematic study of site-specific GalNAc-type O-glycosylation modulating proprotein convertase processing. J Biol Chem. 2011; 286:40122–40132. [PubMed: 21937429]
19. Kato Y. The multiple roles of Notch signaling during left-right patterning. Cellular and Molecular Life Sciences. 2011
20. Lopes SS, et al. Notch signalling regulates left-right asymmetry through ciliary length control. Development. 2010; 137:3625–3632. [PubMed: 20876649]
21. Krebs LT, et al. Notch signaling regulates left-right asymmetry determination by inducing Nodal expression. Genes Dev. 2003
22. Pennekamp P, et al. The ion channel polycystin-2 is required for left-right axis determination in mice. Curr Biol. 2002; 12:938–943. [PubMed: 12062060]
23. Duldulao NA, Lee S, Sun Z. Cilia localization is essential for in vivo functions of the Joubert syndrome protein Arl13b/Scorpion. Development. 2009; 136:4033–4042. [PubMed: 19906870]
24. Raya A, et al. Notch activity acts as a sensor for extracellular calcium during vertebrate left-right determination. Nature. 2004; 427:121–128. [PubMed: 14712268]
25. Stubbs JL, Oishi I, Izpisua Belmonte JC, Kintner C. The forkhead protein Foxj1 specifies node-like cilia in Xenopus and zebrafish embryos. Nat Genet. 2008; 40:1454–1460. [PubMed: 19011629]
26. Bisgrove BW, Makova S, Yost HJ, Brueckner M. RFX2 is essential in the ciliated organ of asymmetry and an RFX2 transgene identifies a population of ciliated cells sufficient for fluid flow. Dev Biol. 2012; 363:166–178. [PubMed: 22233545]
27. Chung MI, et al. RFX2 is broadly required for ciliogenesis during vertebrate development. Dev Biol. 2012; 363:155–165. [PubMed: 22227339]
28. Shinohara K, et al. Two rotating cilia in the node cavity are sufficient to break left-right symmetry in the mouse embryo. Nature communications. 2012; 3:622.
29. Kamura K, et al. Pkd1l1 complexes with Pkd2 on motile cilia and functions to establish the left-right axis. Development. 2011; 138:1121–1129. [PubMed: 21307098]
30. Vick P, et al. Flow on the right side of the gastrocoel roof plate is dispensable for symmetry breakage in the frog Xenopus laevis. Dev Biol. 2009; 331:281–291. [PubMed: 19450574]

Methods References

31. del Viso F, Khokha M. Generating diploid embryos from Xenopus tropicalis. Methods Mol Biol. 2012; 917:33–41. [PubMed: 22956081]
32. Nieuwkoop, PD.; Faber, J. Normal table of Xenopus laevis (Daudin) : a systematical and chronological survey of the development from the fertilized egg till the end of metamorphosis. Garland Pub.; 1994.
33. Khokha MK, et al. Techniques and probes for the study of Xenopus tropicalis development. Dev Dyn. 2002; 225:499–510. [PubMed: 12454926]
34. Vonica A, Brivanlou AH. The left-right axis is regulated by the interplay of Coco, Xnr1 and derriere in Xenopus embryos. Dev Biol. 2007; 303:281–294. [PubMed: 17239842]
35. Caspary T, Larkins CE, Anderson KV. The graded response to Sonic Hedgehog depends on cilia architecture. Dev Cell. 2007; 12:767–778. [PubMed: 17488627]
36. Piperno G, Fulller MT. Monoclonal antibodies specific for an acetylated form of alpha-tubulin recognize the antigen in cilia and flagella from a variety of organisms. J Cell Biol. 1985; 101:2085–2094. [PubMed: 2415535]
37. Schwientek T, et al. Functional conservation of subfamilies of putative UDP-N-acetylgalactosamine:polypeptide N-acetylgalactosaminyltransferases in Drosophila, Caenorhabditis elegans, and mammals. One subfamily composed of l(2)35Aa is essential in Drosophila. J Biol Chem. 2002; 277:22623–22638. [PubMed: 11925450]
38. Pedersen JW, et al. Lectin domains of polypeptide GalNAc transferases exhibit glycopeptide binding specificity. J Biol Chem. 2011; 286:32684–32696. [PubMed: 21768105]
39. Walentek P, Beyer T, Thumberger T, Schweickert A, Blum M. ATP4a is required for Wnt-dependent Foxj1 expression and leftward flow in Xenopus left-right development. Cell reports. 2012; 1:516–527. [PubMed: 22832275]
40. Steentoft C, et al. Mining the O-glycoproteome using zinc-finger nuclease-glycoengineered SimpleCell lines. Nat Methods. 2011; 8:977–982. [PubMed: 21983924]
41. Steentoft C, et al. Precision mapping of the human O-GalNAc glycoproteome through SimpleCell technology. Embo J. 2013; 32:1478–88. [PubMed: 23584533]

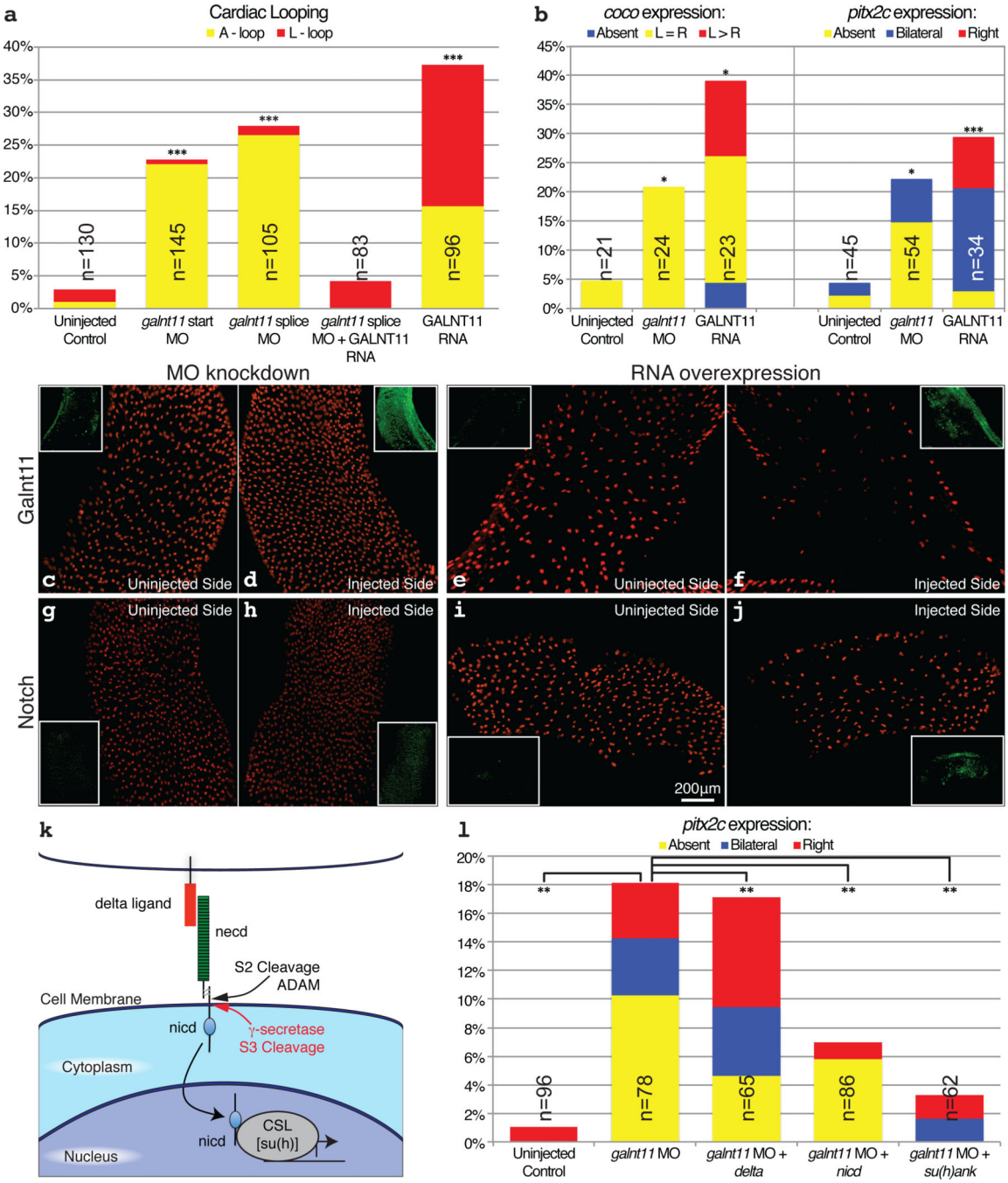

Figure 1. Galnt11 alters LR patterning and Notch signaling

Percent of embryos that have abnormal (a) cardiac looping (either A loops or L loops) or (b) abnormal coco or pitx2c expression L: left, R: right. c–j) *Xenopus* epidermal multiciliated cells marked by anti-acetylated α-tubulin (red). Embryos were injected at the two cell stage targeting the epidermis on either the right or left side with either *galnt11* MO (d), *GALNT11* RNA (f), *notch1* MO (h), or *nicd* RNA (j) and compared to the uninjected side (c, e, g, i). GFP (insets) trace the injected side. All views are lateral views with dorsal to the top. k) Schematic of the Notch pathway l) Percent of embryos with abnormal *pitx2c* in *galnt11*

morphants or *galnt11* morphants co-injected with members of the Notch pathway. Panel (a) UC *n*=130, *galnt11* start MO *n*=145, *galnt11* splice MO *n*=105, *galnt11* splice MO + *galnt11* RNA *n*=83, *galnt11* RNA *n*=96. Panel (b) *coco* expression UC *n*=21, *galnt11* MO *n*=24, *galnt11* RNA *n*=23; *pitx2c* expression UC *n*=45, *galnt11* MO *n*=54, *galnt11* RNA *n*=34. Panel (l) UC *n*=96, *galnt11* MO *n*=78, *galnt11* MO + *delta* *n*=65, *galnt11* MO + *nicd* *n*=86, *galnt11* MO + *su(h)ank* *n*=62. Bars depict means. Additional details are in Methods.

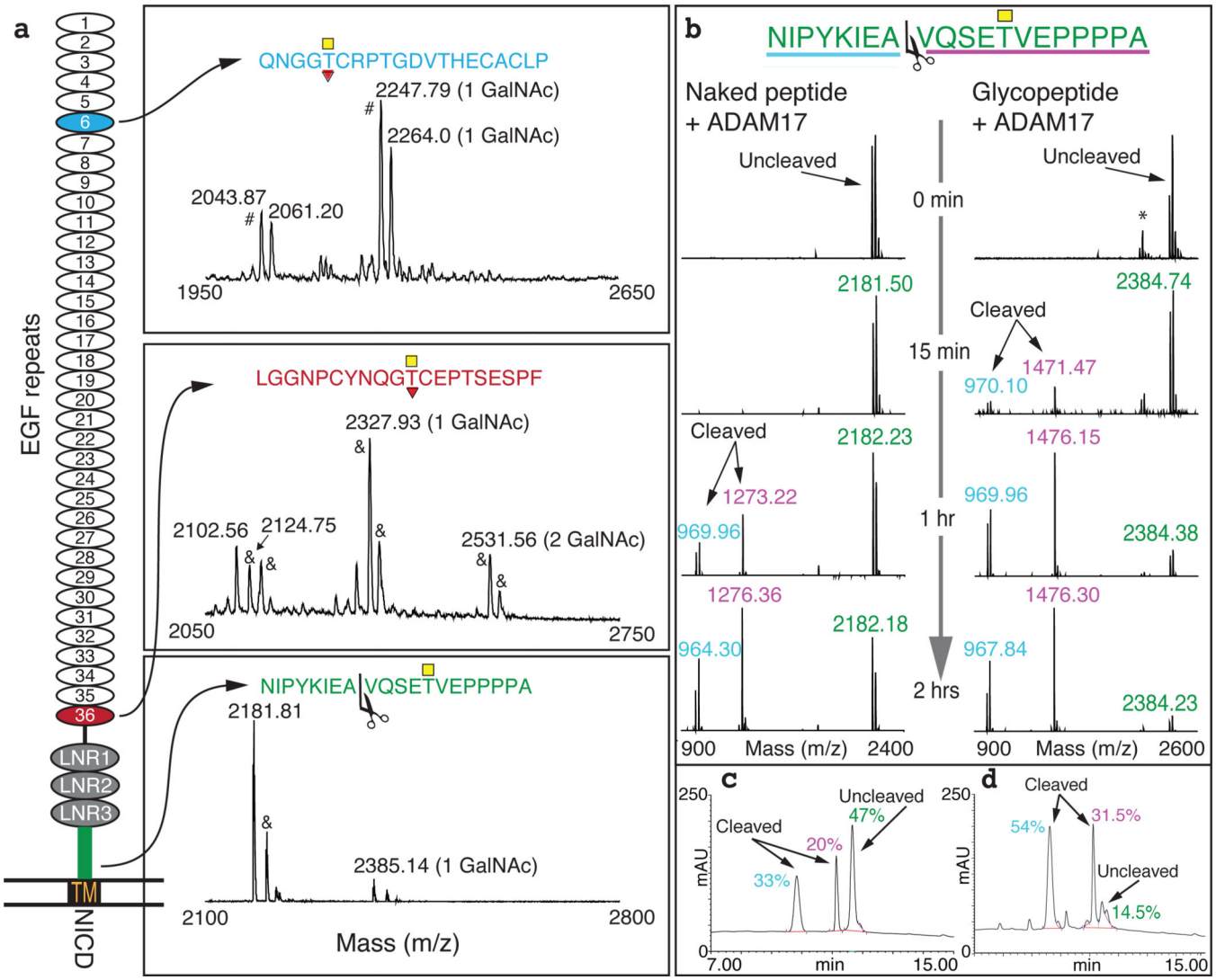

Figure 2. GALNT11 glycosylation of NOTCH1 derived peptides and effects on ADAM-mediated cleavage

a) Depiction of NOTCH1 with MALDI-TOF spectra demonstrating O-GalNAc glycosylation of peptides derived from EGF6 (blue), EGF36 (magenta) and the juxtamembrane region (green). Yellow squares: O-GalNAc, Red triangles: O-Fuc. TM: transmembrane domain; NICD: Notch intracellular domain; # deammoniated peptide; & sodium adducts. b) MALDI-TOF time-course analysis of *in vitro* cleavage of the juxtamembrane peptide and glycopeptide by ADAM17. Scissors: Cleavage site. *nonspecific N-terminal degradation of two amino acids. c–d) HPLC analysis of the cleavage reactions with c) naked peptide and d) glycopeptide after 2 hrs (percentages above the peaks) with $p<0.05$ (two-tailed t-test).

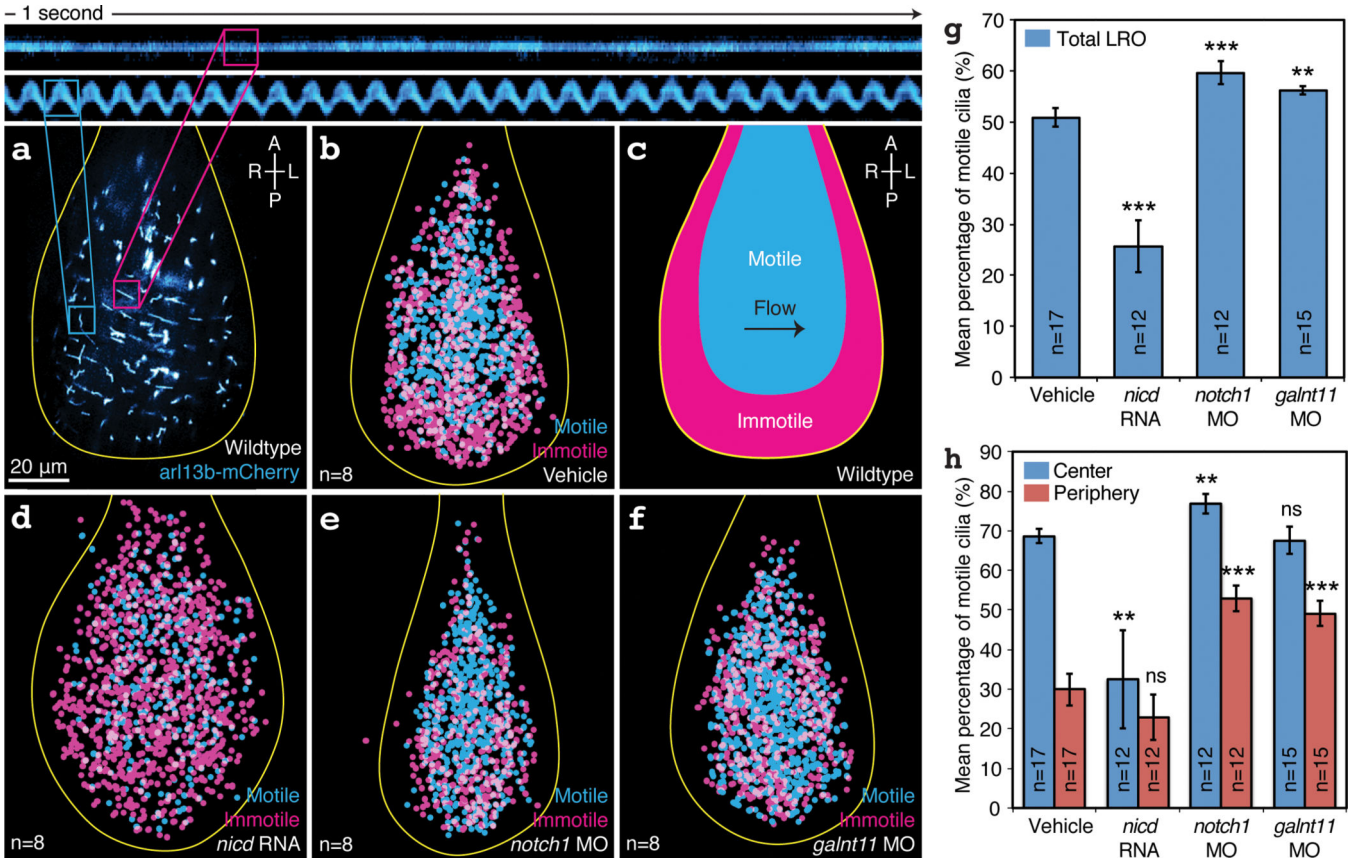

Figure 3. Galnt11/Notch signaling switches cilia between motile and immotile types

a) Wildtype LRO explants expressing *arl13b-mCherry* reveal distinct populations of immotile and motile cilia. Cyan box highlights a single motile cilium, with a corresponding kymograph analyzing beating frequency. Magenta box highlights immotile cilium and kymograph. b) Analysis of multiple vehicle LROs reveals a specific geography for cilia types: immotile cilia are enriched along the fringes, while motile cilia are enriched in the center. c) Schematic of a wildtype LRO A: anterior, P: posterior, L: left, R: right. d) *nicd* overexpressants exhibit a decrease in motile cilia in the center of the LRO. *notch1* (e) and *galnt11* (f) morphants display a decrease in immotile cilia along the LRO periphery. (g–h) Quantification of motile cilia distribution in total LROs (g), and in the center and along the periphery of the LRO (h). Bars depict means and error bars are standard error. b,d,e,f) n=8. g,h) vehicle n=17, *nicd* RNA n=12, *notch1* MO n=12, *galnt11* MO n=15. Additional details are in Methods.